Journal of Quantitative Spectroscopy & Radiative Transfer 113 (2012) 607–623

Contents lists available at SciVerse ScienceDirect

Journal of Quantitative Spectroscopy & Radiative Transfer

journal homepage: www.elsevier.com/locate/jqsrt

Absorption coefficient measurements of particle-laden filters using laser heating: Validation with nigrosin

Cary Presser *

Material Measurement Laboratory, National Institute of Standards and Technology, 100 Bureau Drive, Gaithersburg, MD 20899-8320, USA

ARTICLE INFO

Article history:
Received 18 August 2011
Received in revised form
21 December 2011
Accepted 15 January 2012
Available online 21 January 2012

Keywords:
Absorptivity
Absorption coefficient
Climate change
Laser heating
Nigrosin
Particle-laden filters
Transmissivity

ABSTRACT

A laser-heating technique, referred as the laser-driven thermal reactor, was used in conjunction with laser transmissivity measurements to determine the absorption coefficient of particle-laden substrates (e.g., quartz-fiber filters). The novelty of this approach is that it analyzes a wide variety of specific samples (not just filtered samples) and overcomes measurement issues (e.g., absorption enhancement) associated with other filter-based particle absorption techniques. The absorption coefficient was determined for nigrosin-laden, quartz-fiber filters and the effect of the filter on the absorption measurements was estimated when compared to the isolated nigrosin results. The isolated nigrosin absorption coefficient compared favorably with Lorenz–Mie calculations for an idealized polydispersion of spherical particles (based on a measured nigronsin/de-ionized water suspension size distribution) dispersed throughout a volume equivalent to that of the nigrosin-laden filter. To validate the approach, the absorption coefficient of a nigrosin/de-ionized water suspension was in good agreement with results obtained from an ultraviolet/visible spectrometer. In addition, the estimated imaginary part of the refractive index from the Lorenz–Mie calculations compared well with literature values and was used to estimate the absorption coefficient of optically opaque packed nigrosin.

Published by Elsevier Ltd.

1. Introduction

1.1. Filter-based particle absorption enhancement

The class of filter-based particle absorption techniques (measuring the absorption characteristics of atmospheric aerosol particles collected on filters) include aethalometers, (e.g., Hansen et al. [1]), integrating plate/integrating sphere photometers (e.g., Fry et al. [2], Campbell et al. [3], Lawless et al. [4]), particle soot absorption photometers (e.g., Bond et al. [5]), and multi-angle absorption photometers (e.g., Petzold et al. [6]). Typically, the transmission of light passing through the filter is measured to determine the absorption coefficient in the Beer–Lambert law (or the extinction coefficient when scattering is considered significant). In turn, the absorption coefficient can be related to the imaginary part of the refractive index (depending on the state of the substance, i.e., if a bulk homogeneous substance or aerosolized powder). One important issue that has been reported extensively in the literature (e.g., Campbell et al. [3], Clarke [7], Bohren and Huffman [8], Petzold and Schönlinner [9], Cappa et al. [10]) is the effect of the filter substrate (and possibly the presence of nonabsorbing particles) on determining the correct value for the particle absorption coefficient, often referred to as absorption enhancement (e.g., Taha et al. [11]). This effect is attributed to absorption of backscattered laser light, which on first pass is not absorbed by the particles discretely distributed over and embedded within the fiber filter

* Tel.: +1 301 975 2612.
E-mail address: cpresser@nist.gov

0022-4073/$ - see front matter Published by Elsevier Ltd.
doi:10.1016/j.jqsrt.2012.01.009

Nomenclature

a	fitting parameter for exponential decaying function (see Fig. 5)
A	sample geometric cross-sectional area [m^2]
A^*	absorbance
Bi	Biot Number ($=hL/k_{sam}$)
c	mass specific absorption cross section ($m^2 g^{-1}$)
C	solute/solvent molar concentration ($mol\ L^{-1}$)
$\overline{C}_{ext}$,$\overline{C}_{sca}$,$\overline{C}_{abs}$	mean extinction, scattering, and absorption cross sections, respectively (m^2)
$c_p(T)$	specific heat capacity ($J\ g^{-1}\ K^{-1}$)
$\overline{C}_v$	mean volume fraction
d	characteristic path length through the sample (m)
(dT/dt)	sample temperature derivative ($K\ s^{-1}$)
D	diameter (m)
D_g	geometric mean diameter (m)
D_{32}	volume-to-surface area mean diameter (Sauter mean diameter) (m)
$F(T,T_o)$	heat transfer term (W)
h	convection heat transfer coefficient ($W\ m^{-2}\ K^{-1}$)
I_I	incident radiation intensity ($W\ m^{-2}$)
I_τ	transmitted radiation intensity ($W\ m^{-2}$)
I_β	absorbed radiation intensity ($W\ m^{-2}$)
I_ρ	reflected radiation intensity ($W\ m^{-2}$)
k	imaginary part of the complex refractive index
k_c	coverage factor
k_{sam}	sample thermal conductivity ($W\ m^{-1}\ K^{-1}$)
L	sample characteristic length (m)
$m(t)$	sample mass with respect to time (g)
m_f	sample final mass (g)
m_r	complex refractive index ($=n_r+ik$)
M	particle mass loading ($g\ m^{-2}$)
n	sample number
n_r	real part of the complex refractive index
N	number density (particles m^{-3})
P_I	incident radiation power (see Table 3) (W)
P_τ	transmitted radiation power (see Table 3) (W)
$P(D)$	probability distribution function
$q(T)$	specific heat release rate due to chemical reactions ($W\ g^{-1}$)
Q_{ext}, Q_{sca}, Q_{abs}	differential extinction, scattering, and absorption efficiencies, respectively
$\overline{Q}_{ext}$,$\overline{Q}_{sca}$,$\overline{Q}_{abs}$	mean extinction, scattering, and absorption efficiencies, respectively
$R_1(T_r)$	rate at which heat is transferred from the reactor at temperature T_r (W)
$R_2(T)$	rate of heat loss from the sample (W)
s	standard deviation of the mean
t	time (s)
t_a,t_b	time initiating Regimes 2 and 3, respectively (see Fig. 5) (s)
T	sample temperature (K)
T_{max}, T_o	steady-state sample temperatures defined in Fig. 4 (K)
T_r	reactor temperature (K)
u_c	combined standard uncertainty
x	size parameter ($=\pi D/\lambda$)
y	absorption penetration depth (m)
z	transformation parameter

Greek symbols

α	sample absorption coefficient (m^{-1})
$\beta(T,\lambda)$	spectral hemispherical absorptivity (fraction absorbed of incident radiation intensity)
β_y	differential spectral hemispherical absorptivity
γ	heat transfer parameter ($W\ K^{-1}$)
$\Delta m(t)$	sample mass change after heating (g)
ε	sample extinction coefficient (m^{-1})
ε_m	solute molar cross section ($m^2\ mol^{-1}$)
λ	wavelength (m)
ρ	spectral hemispherical reflectivity (fraction reflected of incident radiation intensity)
ρ_p	mass density ($g\ m^{-3}$)
σ	sample scattering coefficient (m^{-1})
σ_g	geometric mean standard deviation
τ	spectral hemispherical transmissivity (fraction transmitted of incident radiation intensity)
τ^*	temperature-dependent relaxation time (s)

Subscripts

abs	absorption
Reg#	regime
c	clean copper pan
em	electromagnetic (see Table 2)
ext	extinction
f	clean filter
hb	laser heating beam
i	index ($=p, s$)
j	index ($=ext, sca, abs$)
n	isolated nigrosin
nc	nigrosin packed within the copper pan
nf	nigrosin-laden filter
p	isolated particles
ps	particle-laden substrate
pb	laser probe beam
s	clean substrate
sca	scattering
t	thermal (see Table 2)

Superscripts

b	fitting parameter for exponential decaying function (see Fig. 5)

[5,7]. As a result, a substantial increase may occur in the measured particle absorption. As an example of the presence of this effect, Conny [12] measured the transmission through two individual particle-laden, quartz-filter filters and then for the same two filters mounted one upon another for different orientations of the particle-laden surface (i.e., for the coated sides facing upward, downward, and facing one another). A variety of filters, coated with particulate matter from different sources, were analyzed with a thermal optical transmission instrument. The results indicated that the absorbance for the stacked filters was greater than the sum of the individual filters, and thus an enhancement in absorption was detected of up to a factor of about 1.5. Bond and Bergstrom [13] mention in their review of absorption enhancement effects that under certain conditions this effect can be significant (with a correction factor of 3.5).

1.2. Nigrosin for validation of absorption techniques

As reported by the Intergovernmental Panel on Climate Change [14], the major absorbing component of atmospheric aerosol is combustion-generated carbonaceous particles (also referred to as black carbon or soot). The large uncertainties associated with the absorption properties of soot are well documented in the literature, as summarized by Bond and Bergstrom [13]. As an absorbing medium, aerosolized nigrosin has been used in several investigations instead of carbonaceous particles (e.g., Sedlacek and Lee [15]), even though the morphological properties are different. Nigrosin is a mixture of synthetic black dyes used in making India ink. Its chemical formula is reported as $C_{48}N_9H_{51}$ (molecular weight of 753 g mol^{-1}) [5,16], however, other physical and chemical properties are unavailable. The absorption spectrum for nigrosin is broadband from the visible through the near infrared [17–19]. Nigrosin particles are reported to be water-soluble and spherical when aerosolized. Measurements of its refractive index have been published in the literature, as summarized in Table 1. Also, because the nigrosin particles are spherical, the particle optical properties can be evaluated by Lorenz–Mie theory.

A wide range of values for the nigrosin single-scattering albedo, SSA (ratio of the scattering to extinction coefficients) is reported in the literature. The variation is attributed to a variety of factors (e.g., particle size and composition, filter particle loading, and instrument operating conditions) that influence both scattering and absorption measurements. Bond et al. [5] reported SSA values of approximately 0.5 for an aerosolized suspension of nigrosin in de-ionized water. Measurements were obtained with an optical extinction cell and nephelometer operating at 550 nm (absorption was obtained from the difference between the extinction and scattering). It was recognized that this approach has a large uncertainty since the absorption is obtained from the small difference of two large numbers. More recent nigrosin studies report smaller values (less than 0.5) for SSA [10]. Values of 0.06–0.08 were reported at three increasing nigrosin concentrations from extinction/scattering measurements with a pulsed cavity ring-down transmissometer in tandem with a nephelometer at wavelengths of 532 nm and 1064 nm [19,20]. Nigrosin was also used to investigate enhanced absorption effects and derive correction factors for filter-based particle soot absorption photometers (PSAP) [10,16]. Cappa et al. [10] compared the PSAP particle-laden filters to aerosol in a photoacoustic spectrometer. Results indicated that filters loaded with nonabsorbing particles (in addition to the glass filter) can further enhance the absorption of the absorbing component (i.e., nigrosin or soot) on a filter, resulting in a correction larger than a factor of 2. Kondo et al. [16] and Nakayama et al. [21] indicated that the dependency of particle size (comparing PSAP measurements for different monodispersed diameters of nigrosin to Lorenz–Mie theory calculations) influenced the value of the correction factor (larger 600 nm particles brought the correction factor closer to unity while smaller 100–200 nm particles increased the value to 1.9).

1.3. Measuring filter-based particle absorption by laser-heating

In this investigation, a laser-heating technique, referred to historically as the laser-driven thermal reactor (LDTR), was used to estimate (without correction factors) the absorption coefficient of nigrosin particles distributed on a quartz-fiber. The LDTR was used in the past to measure other thermophysical properties of various substances (i.e., energy release, heating value, and reaction kinetics of hazardous wastes and other types of materials [22]); in this study it was used to determine substance absorptivity. The concept involves heating selected particles to a steady-state temperature, perturbing the

Table 1
Value of the refractive index for aerosolized nigrosin from several investigations. CRD – cavity ring down, CW – continuous wave, LSAC – light scattering aerosol counter, PAS – photoacoustic spectrometer ASASP-X – active scattering aerosol spectrometer probe, PTI – photothermal interferometry.

Refractive index ($m_r=n_r+ik$)	Wavelength (nm)	Approach	Reference
$1.67+i0.26$	532	ASASP-X	Garvey and Pinnick [46]
$1.70+i0.31$	532	CRD, PAS	Lack et al. [24]
$1.77+i0.32$	514	PTI	Sedlacek and Lee [15]
$1.649+i0.238$	532	CRD	Dinar et al. [47], Rizik et al. [48]
$1.72+i0.28$	532	CW-CRD	Lang-Yona et al. [49]
$1.65+i0.24$		Pulsed CRD	
$1.693+i0.275$	532		Mean value

temperature with a laser beam that impinges directly on the particles, and monitoring the temperature decay back to the steady state. Substance absorptivity at a given temperature and wavelength is determined using the LDTR time-resolved temperature and a model for energy conservation. The substance absorption coefficient was determined with additional transmissivity measurements. The absorption coefficient was obtained for nigrosin-laden quartz-fiber filters and the effect of the filter on the absorption measurements was estimated when compared to the isolated nigrosin results. Regarding validation of the approach, packed nigrosin samples were evaluated, as well as nigrosin/de-ionized water suspension at different concentrations (with comparison to ultraviolet/visible spectrometer results).

2. Experimental approach

The laser-driven thermal reactor (LDTR) is used to measure rapidly the combined thermal response of a substance, i.e., due to both substance thermal and chemical heat release. One major advantage of this approach is that the absorption coefficient of a variety of samples, e.g., solid particles, liquid droplets, and particle-laden filters, can be estimated directly without the need for correction factors. In this study, we demonstrate that the LDTR approach can overcome absorption enhancement effects associated with current filter-based measurements (e.g., Campbell et al. [3], Clarke [7], Bohren and Huffman [8], Petzold and Schönlinner [9], Bond and Bergstrom [13]), by measuring the filter absorption with and without the sample particles so as to isolate and remove the filter effect from the measurements. In addition, measurements can be carried out also with other non-scattering substrates (or without a substrate) in order to isolate particle absorption. Another advantage is that the LDTR can characterize selected individual samples over a wide range of operating conditions (surrounding temperature, pressure, composition, humidity, etc.). In contrast, extractive laser techniques, for example, photoacoustic spectroscopy (e.g., Arnott et al. [23], Lack et al. [24]), cavity ring down spectroscopy (e.g., Spindler et al. [25]), photothermal interferometry [15], and extinction/scattering (e.g., Schnaiter et al. [26]) depend on ensemble-averaged measurements of particle-laden streams evaluated usually at normal-instrument ambient operating conditions.

2.1. LDTR experimental arrangement

A schematic of the experimental arrangement and supporting sub-systems is presented in Figs. 1 and 2, respectively. The experimental protocol involves using a high-powered laser (operating in the infrared) to heat to a selected steady-state temperature a small copper-foil spherical reactor. The reactor is positioned near the center of a 5 L vacuum chamber containing five viewing ports (four ports on the chamber side placed 90 degrees apart and one port on the top). Sample is placed on, and in contact with, a fine-wire thermocouple that is positioned near the center of the spherical reactor prior to a measurement, and then heated indirectly by the infrared laser. A 'probe' laser beam is then used to heat the sample directly through an opening in the top of the spherical reactor, and perturb the temperature to a new steady-state temperature. The temperature decay is then monitored after the probe beam is blocked, and the experiment is concluded after disengaging the infrared heating beam.

The top of the vacuum chamber provides access to the reactor and is sealed with an o-ring. Each viewing port includes a vacuum-sealed 76 mm diameter quartz window, which is suitable for transmission of the infrared laser beams to the reactor. After softening a piece of copper foil, the reactor is fabricated by pressing the copper into a stainless steel ball-shaped form, which results in a hemisphere. Two pieces are fabricated and placed together to form the sphere. An opening is cut in the top of the sphere (diameter of ≈ 7.2 mm), which allows for placement of the sample and transmission of the probe beam, and another opening in the bottom (diameter of ≈ 4.0 mm) is used to introduce the thermocouples. To precondition the reactor surface, a small nonsooting propane torch is used to heat and generate a copper oxide layer, which reduces laser-beam scattering, surface reactivity, and heat transfer effects that occur if the oxide layer is formed during experiments. Near the center of the copper reactor (with a diameter of (18.2 ± 0.03) mm[1] and thickness of 0.14 mm), sample is placed on and supported by thin-wire extensions that protrude from near the bead of the thermocouple (see Fig. 1). The sample rests on, and is in contact with, a commercially fabricated, K-type, fine-wire thermocouple (0.25 mm in diameter, unsheathed), i.e., 'sample' thermocouple, and a second thermocouple, i.e., 'reactor' thermocouple, is in contact with the reactor inner wall. Embedding the thermocouple within the sample, or having grazing contact, appears to have negligible effect on the reported temperatures. The thermocouple readings are not corrected for radiation effects. The thermocouple time response was estimated to be about 3 s to reach 63.2% of an instantaneous step change in temperature in still ambient air. This value was determined by heating the thermocouple directly with the infrared laser and monitoring the decay in temperature (between 1080 K and 300 K), which was sufficient to resolve the decay in perturbation temperature during the experiments. The expanded uncertainty for the temperature was 2.4 K, including the Type B uncertainty of 1.2 K. Time-resolved temperatures (thermograms) for each thermocouple were recorded with a personal computer/data acquisition system at a rate of three samples s^{-1}.

[1] Estimation of the measurement uncertainty for this study is determined from statistical analysis of a series of replicated measurements (referred to as a Type A evaluation of uncertainty), and from means other than statistical analysis (referred to as a Type B evaluation of uncertainty) [27]. The Type A expanded uncertainty is calculated as $k_c u_c$, where k_c is the coverage factor and u_c is the combined standard uncertainty. The value for u_c is estimated statistically by $sn^{-1/2}$, where s is the standard deviation of the mean and n is the number of samples. For $n=3$ and 5, $k_c=3.18$ and 2.57, respectively, representing a level of confidence of 95%.

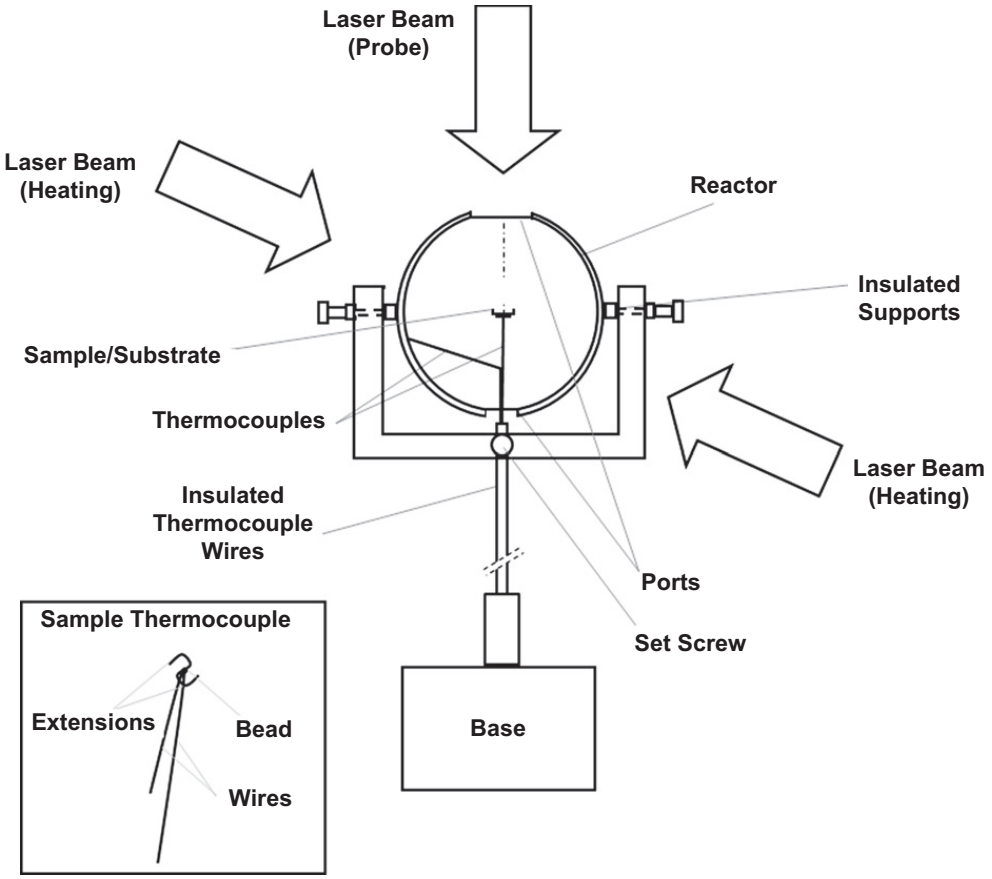

Fig. 1. Schematic of the copper reactor, including the supporting thermocouple and frame.

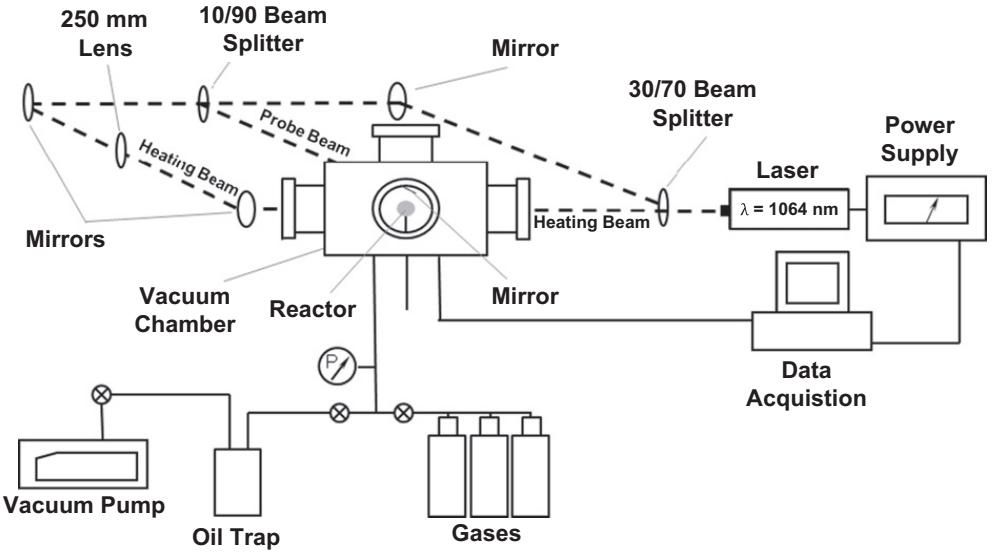

Fig. 2. Schematic of the laser-driven thermal reactor vacuum, optical, and data acquisition sub-systems.

The sample thermocouple and sample are considered to be in thermal equilibrium due to the reactor configuration and the temperature uniformity near the center of the reactor. The nearly uniform sample temperature is maintained by the (1) relative dimensions of the sample and thin-walled sphere, (2) sample alignment in the middle of the sphere, (3) expansion of the laser beam to cover a large portion of the sphere surface, (4) relatively high sphere thermal conductivity ($401\ W\ m^{-1}\ K^{-1}$ at 300 K for copper [28]), and (5) thermal radiation (the dominant mode of heat transfer at high temperature between the interior sphere surface and the sample). Thus, effects due to the laser beam intensity distribution are insignificant. The uniformity in temperature of heating a sample placed within the center of the sphere (for a volume with dimensions of about 10 mm diameter by

5 mm height) is of the order of 1 K [22]. Within the sample, heat transfer is by conduction. The lumped-capacitance approximation [29] is invoked, in which the sample is spatially uniform in temperature at any instant of time during the transient process, as long as the Biot number ($Bi = hL/k_{sam}$) < 0.1 where h is the convection heat transfer coefficient, L is the sample characteristic length (e.g., diameter for spheres or volume-to-surface area ratio for other shapes [29]), and k_{sam} is the sample thermal conductivity. Since experiments are normally carried out under vacuum, the value of h will be negligible ($Bi \ll 0.1$), and thus nonuniformities in temperature over the sample surface and internally will also be negligible.

Heating rates on the order of several hundred Kelvin per second have been achieved for relatively high laser intensities with the LDTR. The apparatus can analyze sample quantities from a few milligrams up to a few grams. The surrounding environment can currently handle a variety of gas compositions, and gas pressures ranging between 10 Pa and 500 kPa. A vacuum pump and manifold are used to obtain vacuum and replace the air in the chamber with other gases, see Fig. 2. Inert gas is used generally to prevent oxidation of volatile matter and other reactions on the sample surface. A Convectron[2] heat-loss pressure gage and controller are used to monitor the vacuum pressure. Additional details of the experimental apparatus are given in Nazarian and Presser [22].

2.2. Nigrosin properties

Samples containing commercially available nigrosin were examined including quartz-fiber filters (inspected visually to be coated and embedded with nigrosin powder), nigrosin powder packed into a copper sample pan, and nigrosin/de-ionized water suspension. The nigrosin density was estimated from the packed nigrosin powder to be 1.13×10^5 g m^{-3}, knowing the nigrosin mass in the pan and the pan volume (see Table 2). Nigrosin was mixed with de-ionized water at four nigrosin molar concentrations of $(0.35,\ 1.47,\ 2.87,\ \text{and}\ 5.54) \times 10^{-5}$ mol L^{-1} $\pm$ 2.9×10^{-8} mol L^{-1}. As stated earlier, nigrosin is generally thought to be water soluble. However, nigrosin is a mixture of different dyes and it is unknown whether all of the dyes are miscible in water. To this end, sample was introduced to a dynamic light scattering (DLS) apparatus (Malvern Zetasizer Nano ZS), which was able to detect both particle size distributions (e.g., see Fig. 3) and the zeta potential. The magnitude of the zeta potential was sufficiently large (mean value of about -50 mV) to indicate that the particles would resist aggregation and remain in suspension. The instrument was set with properties for nigrosin and water dispersant at 293 K, using a 100 μL disposable polystyrene cuvette, 30 s equilibration time, at least 6 runs of 10 s each, measurement

[2] Certain commercial equipment or materials are identified in this publication to specify adequately the experimental procedure. Such identification does not imply recommendation or endorsement by the National Institute of Standards and Technology, nor does it imply that the materials or equipment are necessarily the best available for this purpose.

Table 2
Measured optical properties for nigrosin in a copper pan, and nigrosin coating a quart-fiber filter: m – sample total initial mass, A – sample geometric cross-sectional area, d – sample characteristic length, β_t – measured absorptivity (thermal), β_{em} – absorptivity (electromagnetic), and τ_{em} – measured transmissivity, C_n – isolated nigrosin molar concentration, α_n – isolated nigrosin absorption coefficient. The reflectivity, ρ_{em}, is calculated from Eq. (8). Reported is the experimental mean and expanded uncertainty.

Case	m/A (g m^{-2})	d (10^{-3} m)	β_t ($=\beta_{em}$)	τ_{em}	C_n [a] (mol L^{-1})	α_n (m^{-1})
Clean pan	2552.0 ± 9.3	2.34 ± 0.008	0.066 ± 0.002	0	[b]_	[b]_
Nigrosin/pan (=Isolated nigrosin)	2817.1 ± 10.2 [c] (265.0 ± 1.4)	[d] 2.34 ± 0.008	0.956 ± 0.016	0	$1.50 \times 10^{-1} \pm 1.3 \times 10^{-3}$	$(3.24 \pm 0.21) \times 10^6$
Clean filter	72.8 ± 3.3	1.27 ± 0.042	0.182 ± 0.014	0.0547 ± 0.0034	[b]_	[b]_
Nigrosin/filter	119.5 ± 5.3 [c] (46.8 ± 2.2)	1.27 ± 0.042	0.579 ± 0.058	0.0323 ± 0.0027	$4.89 \times 10^{-2} \pm 3.9 \times 10^{-3}$	394.3 ± 82.5
[e]Nigrosin/ de-ionized water	[f] (≈ 5422.1) [c] $(9.76 \times 10^{-5} \pm 8.8 \times 10^{-7})$	2.34 ± 0.008 [g] (10.1 ± 0.013)	0.081 ± 0.001	0.919 ± 0.0168	$5.54 \times 10^{-5} \pm 2.9 \times 10^{-8}$	6.33 ± 1.98 [g] (5.79 ± 0.54)

[a] Volume derived from columns for m/A and d.
[b] Values are undefined because nigrosin is not present for these cases.
[d] The absorbance is based on $y = 1.16 \times 10^{-6}$ m.
[c] Isolated nigrosin.
[e] Suspension in a copper pan used to obtain β_t, suspension in a polystyrene cuvette used to obtain τ_{em}.
[f] Approximate because mass changing in time while in pan due to water vaporization (based on pan area).
[g] UV/vis spectrometer result.

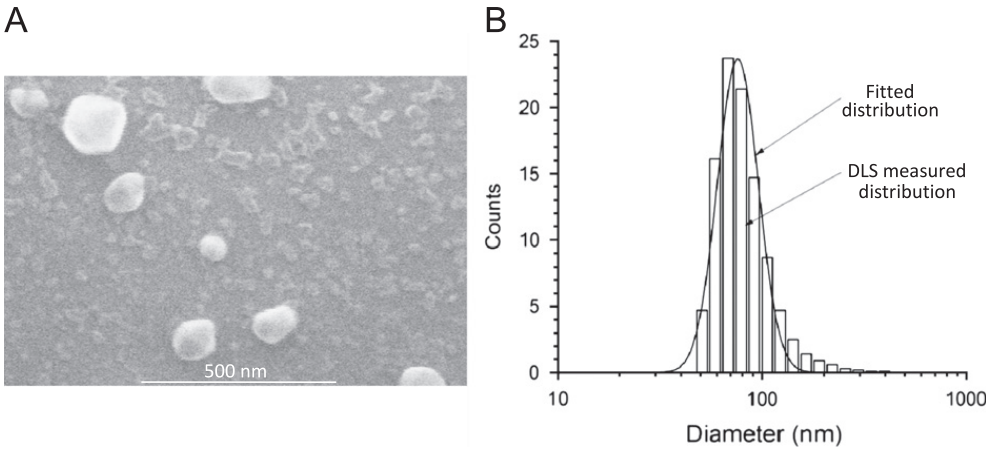

Fig. 3. (A) Conventional field-emission scanning electron microscrope (FE-SEM) image of nigrosin particles (magnification of 363, electron beam energy of 20,000 kV, beam dwell time of 30 μs, horizontal field width of 1.4 μm, pixel size of 1.28 μm for 1024 pixels). (B) Size distribution for the nigrosin/water suspension (molar concentration of 2.41×10^{-5} mol/L) measured using dynamic light scattering (DLS), and a calculated log-normal probability distribution (fitting parameters: $D_g=0.8\times10^{-7}$ m and $\sigma_g=0.23$) using Lorenz–Mie theory.

detection angle of 173°, and wavelength of 633 nm. In addition, suspension was placed on a silicon wafer and dried in the ambient to permit imaging of the particle size and shape with a conventional field-emission scanning electron microscope (FE-SEM, see Fig. 3). The FE-SEM images were obtained at a fixed electron beam energy level of 5 keV and the particles were observed at different magnifications. The particles appear to have diameters similar to those measured with the DLS. Our particle size range was also similar to that formed by Kondo et al. [16] (i.e., 100–600 nm) after they aerosolized, dried, and size-classified (with a tandem differential mobility analyzer) particles from a nigrosin/de-ionized water suspension. The absorbance for our different concentrations of nigrosin/de-ionized water suspension was determined with an ultraviolet/visible (UV/vis) spectrometer (Perkin Elmer Lambda Bio 20 with a 1053 lines/mm holographic concave grating and 1 nm spectral bandpass).

The dimensions of the commercially fabricated round copper pans were (4.95 ± 0.01) mm (inner diameter) $\times$ (2.34 ± 0.008) mm (height) $\times$ (0.125 ± 0.006) mm (thickness). The filters were pure tissue quartz (no binder) punched with a diameter of (7.0 ± 0.1) mm and manufactured with a nominal thickness of (1.27 ± 0.042) mm. The inner length of the polystyrene square cuvette used for the UV/vis spectrometer apparatus was (10.1 ± 0.013) mm.

2.3. Measurement protocol

The sample is heated by an infrared laser beam (which is split into two beams with concomitant beam steering and attenuation optics) and directed to opposing sides of the reactor surface, see Fig. 1. This laser beam is referred to as the 'heating' beam. A 250 W continuous-wave multimode Nd:YAG laser, operating at a wavelength of 1064 nm, is used as the light source for heating the reactor. The sample heating protocol involves an initial heating with the heating beam to a pre-selected steady-state sample temperature. Then direct laser heating of the sample is provided from a third beam (i.e., for this study, a diverted portion of the infrared source beam, referred to as the 'probe' beam) after heating to the steady-state sample temperature (referred to as the 'direct-heating approach' [22]). The probe beam power is measured beforehand inside the chamber with a calibrated power meter. Other sources for the probe beam may also be selected to investigate wavelength-dependent effects. Direct sample heating by the probe beam brings about a small rise in the sample temperature of less than 10% of the steady-state value. This perturbation results in a new steady-state sample temperature (not too different from the original state-state temperature to represent new sample properties). When at this new steady-state temperature, the probe beam is blocked with a beam stop to decrease the sample temperature back to the original steady-state condition. To conclude the experiment, the heating beam is then abated after returning to the original steady-state temperature. The temperature thermogram is then evaluated by the theoretical model described in the next section. The theoretical model is based on the fact that absorption is a process by which incident radiant energy is converted to thermal energy [30], and therefore a theoretical description of substance absorption can be based on both principles of heat transfer and electromagnetism.

2.4. Experimental conditions

Three replicates were recorded of each case, except for the nigrosin/de-ionized water case for which there was 8 replicates. As a means of technique validation, measurements were carried out in air, and for a chamber pressure and steady-state temperature at ambient conditions, to simulate the operating conditions of the nigrosin studies cited earlier (see Table 1). The chamber was open to the environment and thus changes in pressure due to the small temperature rise were not noted. An estimate of the Biot number for nigrosin and for water justified our employment of the lumped-capacitance approximation. Apertures were inserted inside the laser to reduce the laser intensity so as not to damage the copper reactor or samples. Data acquisition was initiated at room

temperature (i.e., the selected steady-state temperature, and thus the heating beam was not used). After 10 s the probe beam was allowed to impinge directly on the sample for approximately 83 s, at which time the probe beam was blocked and the sample temperature returned to the initial steady-state room temperature. Data acquisition was terminated after 150 s. The probe-beam power for the filter, packed, and suspension cases was (2, 13.8, and 162) mW $\pm$ 0.1 mW, respectively.

3. Theoretical model

3.1. Absorption of particle-laden bulk substances by conservation of thermal energy

The theoretical analysis used to determine the absorptivity of a bulk substance involves modeling the decay of the sample temperature after laser heating to a given temperature [22]. The model is representative of samples with a small Biot number [29]. In this limit, where the assumption of a thermally lumped sample temperature is appropriate, the following thermal energy balance governs the heating process:

$$m(t)c_p(T)\mathrm{d}T/\mathrm{d}t = R_1(T_r) - R_2(T) = I_I A\beta(T,\lambda) - F(T,T_o) + \Delta m(t)q(T) \quad (1)$$

where the rate of change of sample internal energy is given by the term on the left side of Eq. (1), $R_1(T_r)$ is the rate at which heat is transferred from the reactor at temperature T_r to the sample, and $R_2(T)$ is the rate of heat loss from the sample, T is the sample temperature, $c_p(T)$ is the sample specific heat capacity at the sample temperature, $m(t)$ is the sample mass with respect to time t. The first term on the right side of Eq. (1) is the energy absorbed by the sample [31], where I_I is the laser beam incident radiation intensity that heats the sample, A is the sample geometric cross-sectional area, $\beta(T,\lambda)$ is the sample hemispherical absorptivity at temperature T and laser wavelength λ. The heat transfer term, $F(T,T_o)$, depends on the sample geometry (defined generically to include arbitrary sample geometries) and represents the sample thermal losses due to conduction and convection (assumed negligible when operating under vacuum) through the gaseous medium, conduction through substrates (e.g., copper support pan used for powders and liquids) and temperature sensor wires, and radiation. The parameter T_o is the sample temperature at steady state (see Fig. 4). Thermal losses due to chemical reaction and vaporization are considered if there is a detectable mass change, $\Delta m(t)$, after heating the sample, with $q(T)$ defined as the specific heat release rate due to chemical reactions.

Eq. (1) is used to describe each regime of the heating protocol (i.e., temperature rise, steady state, and temperature decay), as illustrated by the numbered regimes in Fig. 4. Initially, the sample is heated to a prescribed steady-state temperature (i.e., the temperature at which the sample is evaluated) with the heating beam (Regime 1 in Fig. 4), and is described by Eq. (1). At steady state (within Regime 1), there is no further change in sample temperature (i.e., Eq. (1) with $[m(t)c_p(T)\mathrm{d}T/\mathrm{d}t]_{\mathrm{Reg1}}=0$ where the subscript *Reg#* refers to the corresponding regime). It is expected that any chemical reactions are completed prior to reaching or while maintaining the steady-state temperature in Regime 1 (i.e., before the sample temperature is perturbed by the probe beam, see Fig. 4). Completion of the experiment is represented by the temperature decay back to that of the ambient (Regime 4 in Fig. 4), for which no further incident laser energy is introduced to the sample (i.e., passive response due to the absence of the heating beam; Eq. (1) with $[I_I A]_{\mathrm{Reg4},hb}=0$ where the subscript hb refers to the heating beam). If there is no heat loss and mass change (i.e., no chemical reactions) in Regime 1 then the last term of Eq. (1) is not included in the analysis. The term $q(T)$ is determined after first evaluating the nonreacting regimes 2 and 3 for $\beta(T,\lambda)$ and $F(T,T_o)$, as described next.

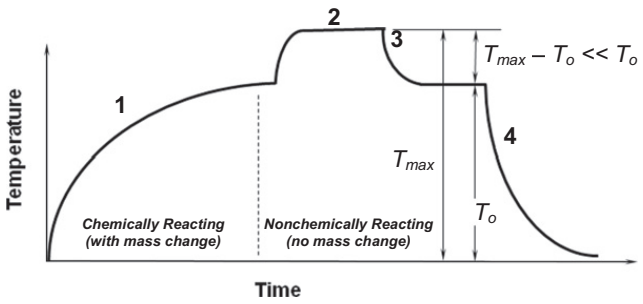

Fig. 4. Schematic of the heating protocol; Regimes: (1) initial heating to the prescribed steady-state temperature, (2) purturbed temperature rise to a new steady-state temperature, (3) temperature decay back to the original steady-state temperature, and (4) termination.

At the steady-state temperature and no further change in mass (end of Regime 1), the probe beam is then directed onto the sample (i.e., with the heating beam still maintaining the steady-state temperature T_o). This causes the sample temperature to rise slightly (within 10% of the original steady-state temperature) to a new steady-state temperature (Regime 2 in Fig. 4). The probe beam is then blocked so that the sample temperature decays to the original steady-state temperature (Regime 3, passive system response due to the absence of the probe beam). Specifically, the two regimes corresponding to the perturbed sample temperature (i.e., Regimes 2 and 3 in Fig. 4, respectively) can be expressed by:

$$\text{temperature rise}: m_f c_p(T)(\mathrm{d}T/\mathrm{d}t)_{\mathrm{Reg2}} = (I_I A)_{\mathrm{pb}}\beta(T,\lambda) - F(T,T_o) \quad (2)$$

$$\text{steady state}: (I_I A)_{\mathrm{pb}}\beta(T,\lambda) = F(T,T_o) \quad (3)$$

$$\text{temperature decay}: m_f c_p(T)(\mathrm{d}T/\mathrm{d}t)_{\mathrm{Reg3}} = -F(T,T_o) \quad (4)$$

where m_f is the sample final mass ($=m(0)-\Delta m(t)$). Note that if the sample does not chemically react (as is the case for this investigation) and the mass remains unchanged ($\Delta m(t)=0$) then $m_f=m(0)$. The subscript "pb" refers to the probe beam.

Analytically, the expression for $F(T,T_o)$ will contain both a conductive (with a T dependence) and radiation (with a T^4 dependence) heat transfer term [22]. Separating variables and integrating Eq. (4), and considering that both conduction and radiation heat transfer contribute to

the sample heat losses, results in a complex exponential expression (a power-law expression results if radiation losses are dominant) for the temperature decay with respect to time. For simplicity, however, we assume an exponentially decaying expression of the form:

$$T-T_o=(T_{\max}-T_o)e^{(-t/\tau^*)} \tag{5}$$

which is numerically similar to the more complicated exponential and power-law functions (since it fits satisfactorily the experimental data) in the regions of interest. The temperature-dependent relaxation time (τ^*) is determined by rearranging Eq. (5). Taking the derivative of Eq. (5) with respect to time at the sample temperature, Eq. (4) can be rewritten as:

$$\gamma(T-T_o)_{\mathrm{Reg3}}=F(T,T_o) \tag{6}$$

where $\gamma=c_p(T)\ m_f/\tau^*$.

Using Eqs. (2)–(4), we solve for the absorptivity, $\beta(T,\lambda)$, with the following protocol. With regression analysis of the measured sample thermogram, an estimate of the best exponentially decaying expression is obtained (a generic example is given in Fig. 5(A) and (B) for the pan at a high steady-state temperature; Fig. 5(C) is a sample from this study at ambient conditions), and of the three fitting parameters, i.e., τ^*, T_o, and $T_{\max}$ (where $\tau^*>0$ and $T_o<T_{\max}$). The temperature derivative $\mathrm{d}T/\mathrm{d}t$ in Eq. (4) is then determined for Regime 3. Mathematically, this derivative (slope) is evaluated at the intercept of the thermogram temperature at $t=0$ in Regime 3, i.e., for $T=T_{\max}$ when initiating the temperature decay. The sample mass is determined using a commercial precision mass balance, and the value of the specific heat capacity is calculated at $T_{\max}$. The value of c_piT) is based on taking the weighted mean from algebraic expressions of $c_p(T)$ (i.e., regressive fits of the data found in Ref. [28]) for the sample (i.e., graphite since values are unavailable for nigrosin, and water) and substrate (i.e., either CuO or SiO_2) used in this investigation. One can then evaluate the heat transfer term, $F(T,T_o)$, at $T_{\max}$ with Eq. (6). For the current study, the aforementioned analytical expressions for $F(T,T_o)$ [22] were not invoked to determine the contribution of each heat transfer mode. It then follows from Eq. (6) that $\beta(T,\lambda)$ at both $T_{\max}$ and λ can be determined knowing the probe-beam laser power (which is precalibrated at the sample location). Equating Eqs. (3), (4), and (6) provides the following useful expression for the absorptivity:

$$\begin{aligned}\beta(T,\lambda)&=-c_p(T_{\max})m_f(\mathrm{d}T/\mathrm{d}t)_{\mathrm{Reg3},T_{\max}}/(I_IA)_{\mathrm{pb}}\\&=-\gamma_{T_{\max}}(T_{\max}-T_o)/(I_IA)_{\mathrm{pb}}\end{aligned} \tag{7}$$

where the mass weighted value of c_p is evaluated at $T_{\max}$. This procedure can be repeated at different laser fluences (i.e., steady-state sample temperatures). Equation (2) can then be used to check for consistency.

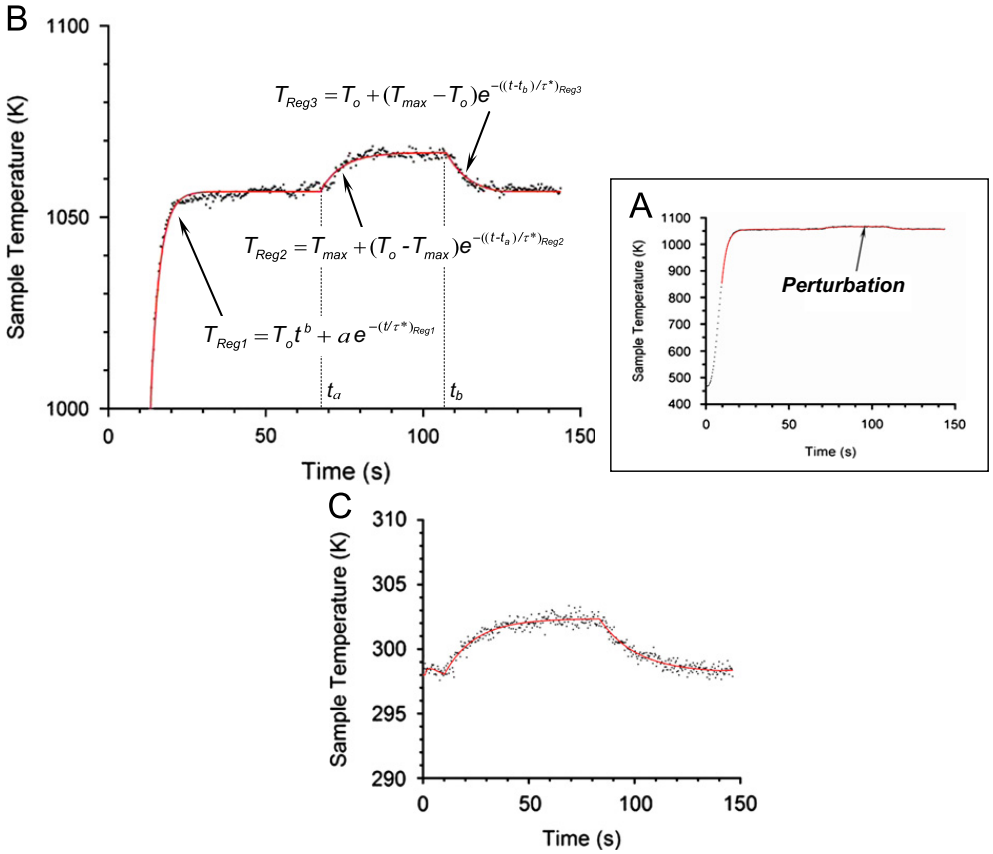

Fig. 5. Sample experimental run (A) and expanded view (B) for the copper pan at high temperature. Data were fit with exponentially decaying functions for regression modeling (given for Regimes 1, 2, and 3, see Fig. 4). The equation for T_{Reg3} is Eq. (5). The power-law term (first term) in the equation for T_{Reg1} is the regression fit for the thermogram steady-state temperature T_o before and after the temperature perturbation. Equating functions of adjoining regions allows for determining the transition time from one region to the next. Regression of the data is not carried out for Regime 4. (C) Experimental run for the copper pan at ambient steady-state temperature (conditions for this study).

3.2. Absorption of particle-laden bulk substances by conservation of electromagnetic radiation

In order to determine the absorption coefficient of a bulk substance, another approach is used (in conjunction with the LDTR results for absorptivity) that is based on the transmission of radiation through a plane-parallel portion of arbitrary homogeneous bulk substance [8,32]. The analysis is dependent on the conservation of incident radiation at a surface, as illustrated in Fig. 6(A), and is expressed as:

$$\rho+\tau+\beta=1 \tag{8}$$

where ρ is the sample spectral hemispherical reflectivity, τ is the sample spectral hemispherical transmissivity, and β is the sample spectral hemispherical absorptivity (near surface phenomenon for opaque substances) [29]. If ρ is the fraction of incident radiation intensity that is reflected, then it follows from Fig. 6(A) that:

$$\rho=I_\rho/I_I \tag{9}$$

$$\tau=I_\tau/I_I=(1-\rho)^2e^{-\varepsilon d} \tag{10}$$

and from Eq. (8):

$$\beta=I_\beta/I_I=1-\rho-(1-\rho)^2e^{-\varepsilon d} \tag{11}$$

where I_ρ is the reflected intensity, I_τ is the transmitted intensity, and I_β is the resulting intensity absorbed by the sample, ε is the extinction coefficient ($\varepsilon\equiv\alpha+\sigma$ [8,32]), d is a known characteristic path length through the sample, and α and σ are the absorption and scattering coefficients, respectively. Higher-order surface reflections (and resulting transmission internal to the sample) are considered negligible [8,29], regardless of the sample. Note that Eq. (11) represents the total cumulative absorptivity through the sample, and can also be derived by specifying the differential absorptivity, integrating over the substance thickness (i.e., path length), and accounting for reflected radiation off of the surface at d (see Fig. 6(A)). Similarly, for the special case of $\tau=0$ (an optically opaque substance), one can estimate the distance absorbed radiation penetrates into the sample by defining the differential absorptivity, β_y, as:

$$\beta_y=\beta(1-e^{-\alpha y}) \tag{12}$$

where y is the absorption penetration depth (distance within the sample normal to the incident surface, see Fig. 6(B)). For $\beta_y\longrightarrow\beta$, the exponential term in Eq. (12) will approach 0. If one knows α, then one can estimate the absorption penetration depth (as indicated in Fig. 6(B)) by rearranging Eq. (12), determining the expanded uncertainty for the quotient β_y/β through propagation of errors, assuming that the combined standard uncertainty for β_y equals that for β, and integrating over y until the estimate for β_y is statistically indistinguishable from β (i.e., $\beta_y=\beta$), then:

$$y=-\frac{1}{\alpha}\ln\left[\frac{\sqrt{2}k_cu_c(\beta)}{\beta}\right] \tag{13}$$

where k_c is the coverage factor, and $u_c(\beta)$ is the combined standard uncertainty of β.

Relating the absorptivity from Eqs. (8) to (7) results in the following useful expression that relates the two above-mentioned approaches:

$$-c_p(T_{\max})m_f(\mathrm{d}T/\mathrm{d}t)_{\mathrm{Reg3},T_{\max}}=(I_\beta A)_{\mathrm{pb}}=[(I_I-I_\rho-I_\tau)A]_{\mathrm{pb}} \tag{14}$$

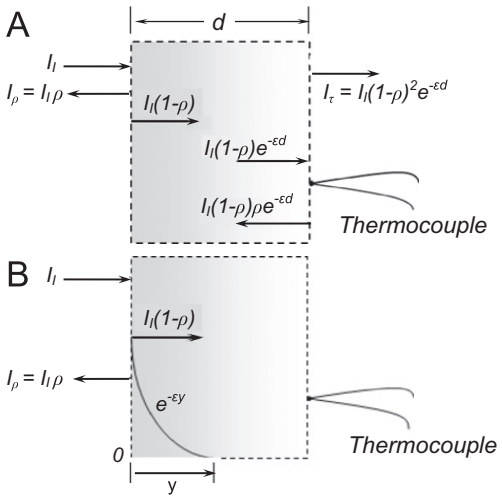

Fig. 6. (A) Transmission of incident electromagnetic radiation through a homogeneous bulk substance. (Higher order surface reflections and related transmissions are considered negligible.) (B) Absorption of radiation within a substance for no transmission ($\tau=0$).

3.3. Particle absorption coefficient for particle-laden substrates

The protocol for determining the absorption coefficient of a particle-laden substrate (e.g., quartz-fiber filter) also requires knowing the value for ρ, as well as that for ε. Thus for closure, in addition to measurement of the absorptivity (using the LDTR approach), the transmissivity is also determined for both the particle-laden substrate and a clean substrate (reference for isolating the particle characteristics). Measurement of the absorptivity is carried out as outlined above, and the transmissivity is measured in-situ with a slightly modified arrangement, as illustrated in Fig. 7, using an additional detector to determine the transmitted beam intensity. With

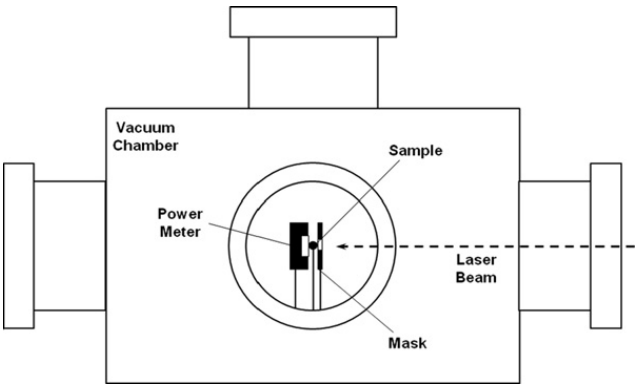

Fig. 7. Schematic of optical arrangement for measuring the sample transmissity.

measurements for both β and τ, the reflectivity is determined from Eq. (8), and the extinction coefficient can be determine from

$$\varepsilon = -\frac{1}{d}\ln\left[\frac{\tau}{(1-\rho)^2}\right] = -\frac{1}{d}\ln\left[\frac{1-\rho-\beta}{(1-\rho)^2}\right] \tag{15}$$

for $\tau > 0$.

To obtain the particle absorption coefficient, α, for a substrate laden with absorbing particles (i.e., particles coating and embedded within the substrate), several conditions need to be satisfied. Since the value of ε must be greater than 0, the following relationships must be satisfied after the measurements are carried out (see Eq. (15)), i.e., $\tau \le (1-\rho)^2$ and $\beta \ge \rho\,(1-\rho)$. We distinguish between the particle-laden substrate and clean substrate with

$$\beta_{ps} = \beta_p + \beta_s \tag{16}$$

and

$$\tau_{ps} = \tau_p \cdot \tau_s = e^{-A^*_{ps}} = e^{-(A^*_p + A^*_s)} \tag{17}$$

where A^* is the absorbance ($A^*_i = \varepsilon_i d = -\ln(\tau_i)$, $i=p, s$), and the subscripts ps, s and p refer to the particle-laden substrate, clean substrate, and isolated particles, respectively. It is assumed that $\beta_{ps} \ge \beta_s$ since the particles are considered absorbing, and thus the measurements should reflect this condition. For the clean substrate, it is expected that $\alpha_s \ll 1$ (and $\beta_s \ll 1$) and therefore $\varepsilon_s = \sigma_s$. The extinction coefficient for the isolated particles is then derived from $\varepsilon_p = \varepsilon_{ps} - \varepsilon_s$ for $\varepsilon_{ps} \ge \varepsilon_s$. Since $\varepsilon_p \equiv \alpha_p + \sigma_p$, then $\varepsilon_p = \alpha_p$ if the particle scattering is negligible, i.e., $\sigma_p \ll 1$.

When considering bulk substances, the absorption coefficient is assumed to be represented by homogeneous, unbounded media [8]:

$$\alpha = 4\pi k/\lambda \tag{18}$$

where k is the imaginary part of the complex refractive index. Note the dependence of refractive index on wavelength and temperature when there are changes in substance composition and morphology. Also, the particle scattering coefficient, σ_p, can be determined by subtracting Eq. (18) from Eq. (15).

Often in the literature for particle-laden filters (e.g., Liousse et al. [33], Weingartner et al. [34]), the sample absorbance, A^*, is reported on a mass specific basis such that $A^* = cM = c\rho_p d$, where c is the mass specific absorption cross section ($m^2\,g^{-1}$), M is the particle mass loading ($g\,m^{-2}$), and ρ_p is the mass density (concentration) ($g\,m^{-3}$). For particle suspensions in liquid, the transmission law is expressed as:

$$\tau = e^{-A^*} = e^{-\varepsilon_m C d} \tag{19}$$

where ε_m is the molar cross section and C is the molar concentration. For dilute suspensions ($A^* < 1$ depending on wavelength [35] or $C < 0.01$ mol L^{-1} [36,37]), the relationship between the absorbance and concentration is linear, whereas for denser concentrations, linearity is affected by particle interactions (including possible changes to the effective refractive index, chemical reactions, etc.), and thus absorbance will become nonlinear with increasing concentration.

4. Results and discussion

Filter-based measurements were carried out under ambient conditions for clean (reference) and nigrosin-laden quartz fiber filters. Validation experiments were carried out for a clean copper pan (reference), the pan packed with nigrosin, and a pan filled with nigrosin/de-ionized water suspension. The measurement results (i.e., absorptivity and transmissity) for the above-mentioned cases are presented in Table 2. Table 3 presents the input data and other relevant information used in determining the values of β and τ. The reported expanded uncertainties are Type A evaluations, which are estimated by determining the standard uncertainty for the variables (see Eq. (7)), completing a propagation of errors analysis, and combining of uncertainties to provide the expanded uncertainty.

4.1. Absorption coefficient measurements of nigrosin-laden quartz filters

The absorptivity and transmissivity for the nigrosin-laden quartz filters are presented in Table 2. It is assumed from observation of the filters that the nigrosin particles are dispersed nonhomogeneously over the surface and embedded within the quartz-fiber filter (considered semi-transparent). Also, no change to the filter properties was expected since the experiments were carried out at ambient conditions. Thus, the path length was derived from the filter thickness. The value of the nigrosin absorption coefficient was estimated from Eq. (15) to be $\varepsilon_n = \alpha_n = (3.94 \pm 0.83) \times 10^2\ m^{-1}$ ($\tau_n = 0.590 \pm 0.061$, $\beta_n = 0.397 \pm 0.060$, $d = (1.27 \pm 0.04) \times 10^{-3}$ m, assuming that $\sigma_n = 0$, and removing the influence of the filter as given in Eqs. (16) and (17)).

As mentioned earlier, these measurements are based on two assumptions, i.e., (1) the nigrosin particles do not scatter ($\sigma_n = 0$), and (2) it is appropriate to determine the isolated nigrosin absorption coefficient by removing the contribution of the clean filter from the nigrosin/filter measurements. To verify these assumptions, the absorption and scattering coefficients were calculated using Lorenz–Mie theory [38] for an idealized polydispersion of non-aggregated, spherical nigrosin particles that were well-dispersed within a volume comparable to that of the filter [8]. The calculations were carried out for an assumed nigrosin refractive index $m_{r,n} = 1.693 + i0.275$ (corresponding to the values reported in Table 1) and wavelength $\lambda = 1.064 \times 10^{-6}$ m. An assumed polydispersion size distribution, represented by a log-normal probability function (see Appendix A), was fitted to the measured particle size distribution for a nigrosin/de-ionized water suspension with a molar concentration of 2.41×10^{-5} mol L^{-1} (the measured size distribution was obtained with the aforementioned dynamic light scattering apparatus using the value of $m_{r,n}$ given above and $A^*_{,n}$ from the UV/Vis spectrometer for λ, see Fig. 8). The reported DLS mean particle size distribution is presented in Fig. 3(B) along with the fitted size distribution for $\tau_n = 0.590$ and $d = 1.27 \times 10^{-3}$ m (see Table 2), and the probability function fitting parameters: $D_g = 0.8 \times 10^{-7}$ m (geometric mean diameter) and $\sigma_g = 0.23$

Table 3
Input values and other relevant parameters used in determining the absorptivity and transmissivity. Reported is the measurement mean and standard uncertainty.

Parameter	Clean filter	Nigrosin/filter	Clean pan	Nigrosin/pan	Nigrosin/de-ionized water/pan
Absorptivity measurements					
c_p [J g^{-1} K^{-1}]	$7.41\times10^{-1}\pm1.0\times10^{-4}$ $7.41\times10^{-1}\pm1.0\times10^{-4}$ $7.41\times10^{-1}\pm1.0\times10^{-4}$	$7.39\times10^{-1}\pm1.0\times10^{-4}$ $7.39\times10^{-1}\pm1.0\times10^{-4}$ $7.39\times10^{-1}\pm1.0\times10^{-4}$	$5.32\times10^{-1}\pm1.0\times10^{-4}$ $5.32\times10^{-1}\pm1.0\times10^{-4}$ $5.32\times10^{-1}\pm1.0\times10^{-4}$	$5.55\times10^{-1}\pm1.0\times10^{-4}$ $5.55\times10^{-1}\pm1.0\times10^{-4}$ $5.55\times10^{-1}\pm1.0\times10^{-4}$	$1.10\times10^{0}\pm1.0\times10^{-4}$ $1.10\times10^{0}\pm1.0\times10^{-4}$ $1.10\times10^{0}\pm1.0\times10^{-4}$ $1.10\times10^{0}\pm1.0\times10^{-4}$ $1.10\times10^{0}\pm1.0\times10^{-4}$ $1.10\times10^{0}\pm1.0\times10^{-4}$ $1.10\times10^{0}\pm1.0\times10^{-4}$ $1.10\times10^{0}\pm1.0\times10^{-4}$
[a]m [g]	$2.8\times10^{-3}\pm1.0\times10^{-5}$	$4.6\times10^{-3}\pm1.0\times10^{-5}$	$4.91\times10^{-2}\pm1.0\times10^{-5}$	$5.42\times10^{-2}\pm1.0\times10^{-5}$	$6.04\times10^{-2}\pm1.0\times10^{-5}$
[a]P_l [W]	$2.0\times10^{-3}\pm1.0\times10^{-4}$	$2.0\times10^{-3}\pm1.0\times10^{-4}$	$1.38\times10^{-2}\pm1.0\times10^{-4}$	$1.38\times10^{-2}\pm1.0\times10^{-4}$	$1.62\times10^{-1}\pm1.0\times10^{-4}$
dT/dt [K s^{-1}]	$-1.34\times10^{-1}\pm6.2\times10^{-4}$ $-2.25\times10^{-1}\pm5.6\times10^{-3}$ $-9.82\times10^{-2}\pm4.3\times10^{-3}$	$-3.18\times10^{-1}\pm7.6\times10^{-5}$ $-3.53\times10^{-1}\pm9.9\times10^{-5}$ $-3.50\times10^{-1}\pm9.7\times10^{-5}$	$-2.55\times10^{-2}\pm2.4\times10^{-4}$ $-5.99\times10^{-2}\pm4.3\times10^{-3}$ $-1.89\times10^{-2}\pm2.9\times10^{-4}$	$-4.50\times10^{-1}\pm2.3\times10^{-3}$ $-4.27\times10^{-1}\pm7.4\times10^{-5}$ $-3.67\times10^{-1}\pm5.9\times10^{-5}$	$-1.07\times10^{-1}\pm7.2\times10^{-5}$ $-1.22\times10^{-1}\pm1.2\times10^{-4}$ $-1.39\times10^{-1}\pm7.3\times10^{-5}$ $-1.45\times10^{-1}\pm6.9\times10^{-5}$ $-1.66\times10^{-1}\pm9.3\times10^{-5}$ $-2.50\times10^{-1}\pm1.5\times10^{-4}$ $-2.83\times10^{-1}\pm6.8\times10^{-5}$ $-3.67\times10^{-1}\pm1.2\times10^{-4}$
T_o [K]	$297.9\pm5.3\times10^{-6}$ $297.3\pm1.7\times10^{-5}$ $298.0\pm7.0\times10^{-5}$	$298.0\pm3.3\times10^{-6}$ $298.0\pm3.4\times10^{-6}$ $298.0\pm3.5\times10^{-6}$	$297.4\pm7.7\times10^{-6}$ $297.5\pm1.9\times10^{-5}$ $297.7\pm4.6\times10^{-6}$	$298.6\pm7.3\times10^{-6}$ $298.8\pm3.8\times10^{-6}$ $298.9\pm3.7\times10^{-6}$	$289.6\pm1.9\times10^{-4}$ $291.8\pm1.9\times10^{-4}$ $292.5\pm8.5\times10^{-5}$ $293.6\pm6.5\times10^{-5}$ $294.8\pm5.6\times10^{-5}$ $297.0\pm3.6\times10^{-5}$ $295.8\pm3.6\times10^{-5}$ $296.4\pm5.7\times10^{-5}$
$T_{\max}$ [K]	$298.8\pm1.5\times10^{-5}$ $298.7\pm4.3\times10^{-5}$ $298.7\pm1.3\times10^{-4}$	$302.9\pm9.9\times10^{-6}$ $302.9\pm1.0\times10^{-5}$ $302.9\pm1.0\times10^{-5}$	$298.0\pm1.9\times10^{-5}$ $298.2\pm3.5\times10^{-5}$ $298.0\pm1.2\times10^{-5}$	$305.1\pm1.4\times10^{-5}$ $305.0\pm1.0\times10^{-5}$ $304.9\pm1.0\times10^{-5}$	$301.9\pm3.8\times10^{-4}$ $302.3\pm3.7\times10^{-4}$ $302.9\pm1.7\times10^{-4}$ $303.0\pm1.3\times10^{-4}$ $303.4\pm1.1\times10^{-4}$ $305.2\pm6.9\times10^{-5}$ $307.4\pm6.8\times10^{-5}$ $309.2\pm1.1\times10^{-4}$
τ^* [s]	$6.75\times10^{0}\pm6.7\times10^{-5}$ $6.16\times10^{0}\pm5.0\times10^{-4}$ $7.73\times10^{0}\pm6.1\times10^{-4}$	$1.55\times10^{1}\pm4.3\times10^{-5}$ $1.37\times10^{1}\pm4.4\times10^{-5}$ $1.39\times10^{1}\pm4.4\times10^{-5}$	$2.34\times10^{1}\pm3.1\times10^{-4}$ $1.25\times10^{1}\pm1.6\times10^{-3}$ $2.12\times10^{1}\pm3.1\times10^{-4}$	$1.45\times10^{1}\pm1.1\times10^{-3}$ $1.45\times10^{1}\pm3.6\times10^{-5}$ $1.65\times10^{1}\pm3.8\times10^{-5}$	$1.16\times10^{2}\pm2.3\times10^{-3}$ $8.76\times10^{1}\pm2.2\times10^{-3}$ $7.49\times10^{1}\pm9.7\times10^{-4}$ $6.49\times10^{1}\pm6.9\times10^{-4}$ $5.16\times10^{1}\pm5.9\times10^{-4}$ $3.28\times10^{1}\pm3.8\times10^{-4}$ $4.09\times10^{1}\pm2.6\times10^{-4}$ $3.48\times10^{1}\pm3.3\times10^{-4}$
n	81 29	196 189	124 149	184 184	169 183

	91	184	170	167	187 177 186 130 129 137
β_t	$0.139 \pm 1.1 \times 10^{-3}$ $0.305 \pm 9.8 \times 10^{-3}$ $0.102 \pm 4.5 \times 10^{-3}$	$0.540 \pm 2.7 \times 10^{-2}$ $0.600 \pm 3.0 \times 10^{-2}$ $0.596 \pm 3.0 \times 10^{-2}$	$0.048 \pm 5.7 \times 10^{-4}$ $0.113 \pm 8.2 \times 10^{-3}$ $0.036 \pm 6.1 \times 10^{-4}$	$0.981 \pm 8.7 \times 10^{-3}$ $0.931 \pm 6.7 \times 10^{-3}$ [b]$0.799 \pm 5.8 \times 10^{-3}$	$0.044 \pm 4.1 \times 10^{-5}$ $0.050 \pm 5.6 \times 10^{-5}$ $0.057 \pm 4.8 \times 10^{-5}$ $0.060 \pm 4.8 \times 10^{-5}$ $0.068 \pm 5.8 \times 10^{-5}$ $0.103 \pm 9.1 \times 10^{-5}$ $0.117 \pm 8.0 \times 10^{-5}$ $0.151 \pm 1.1 \times 10^{-4}$

Parameter	Clean filter	Nigrosin/filter	Clean pan	Nigrosin/pan	Nigrosin/de-ionized water/cuvette
Transmissivity measurements					
P_l (W)	[c]$6.0 \times 10^{-3} \pm 1.1 \times 10^{-4}$ $2.9 \times 10^{-2} \pm 3.5 \times 10^{-4}$ $5.3 \times 10^{-2} \pm 1.3 \times 10^{-4}$	[c]$6.0 \times 10^{-3} \pm 1.1 \times 10^{-4}$ $2.9 \times 10^{-2} \pm 3.5 \times 10^{-4}$ $5.3 \times 10^{-2} \pm 1.3 \times 10^{-4}$	[d]–	[d]–	[e]$1.9 \times 10^{-1} \pm 7.7 \times 10^{-4}$
P_τ (W)	[c]$3.0 \times 10^{-4} \pm 1.7 \times 10^{-6}$ $1.8 \times 10^{-3} \pm 1.0 \times 10^{-5}$ $2.8 \times 10^{-3} \pm 1.4 \times 10^{-4}$	[c]$2.5 \times 10^{-4} \pm 1.0 \times 10^{-5}$ $9.0 \times 10^{-4} \pm 3.7 \times 10^{-5}$ $1.3 \times 10^{-3} \pm 1.2 \times 10^{-5}$	[d]–	[d]–	[e,f]$1.5 \times 10^{-1} \pm 7.1 \times 10^{-4}$ [e,g]$1.1 \times 10^{-1} \pm 5.5 \times 10^{-4}$

[a] Values are the same for all experiments.
[b] Outlier and not considered further.
[c] The three values (average values for five measurements) correspond to three different laser fluencies.
[d] No transmission occurs through the pan.
[e] Average value for five measurements.
[f] Average value for the transmission through the cuvette.
[g] Average value for the transmission through the cuvette with sample.

(geometric mean standard deviation). The transmissivity for a polydispersion of spherical particles is given by [39–41]:

$$\tau = e^{-\varepsilon d} = e^{-N\overline{C}_{ext}d} = e^{-(3\overline{Q}_{ext}\overline{C}_v d/2D_{32})} \quad (20)$$

where N is the number density, $\overline{C}_{ext}(=\overline{C}_{sca}+\overline{C}_{abs})$ is the mean extinction cross section, $\overline{Q}_{ext}(=\overline{Q}_{sca}+\overline{Q}_{abs})$ is the mean extinction efficiency, $\overline{C}_v$ is the volume fraction, and D_{32} is the volume-to-surface area diameter. Pertinent details for evaluating the terms in Eq. (20) are given in Appendix A. The computational results were $\varepsilon_n=414.8\ m^{-1}$, $\sigma_n=20.3\ m^{-1}$, $\alpha_n=394.5\ m^{-1}$ (SSA=0.049, see Table 4). These results indicate that the isolated nigrosin absorption coefficient for the nigrosin-laden filter absorptivity/transmissivity experiments (see Table 2) was similar to the value calculated for the idealized dispersion of nigrosin particles. The nigrosin scattering coefficient is less than 5% of the extinction coefficient and can be considered negligible, as assumed earlier. In addition, these results indicate that the absorption was not dependent on the spatial particles dispersion throughout the filter volume (i.e., no apparent effect of the nonhomogenous particles distribution within the filter, although the theory was based on a homogenous particles distribution).

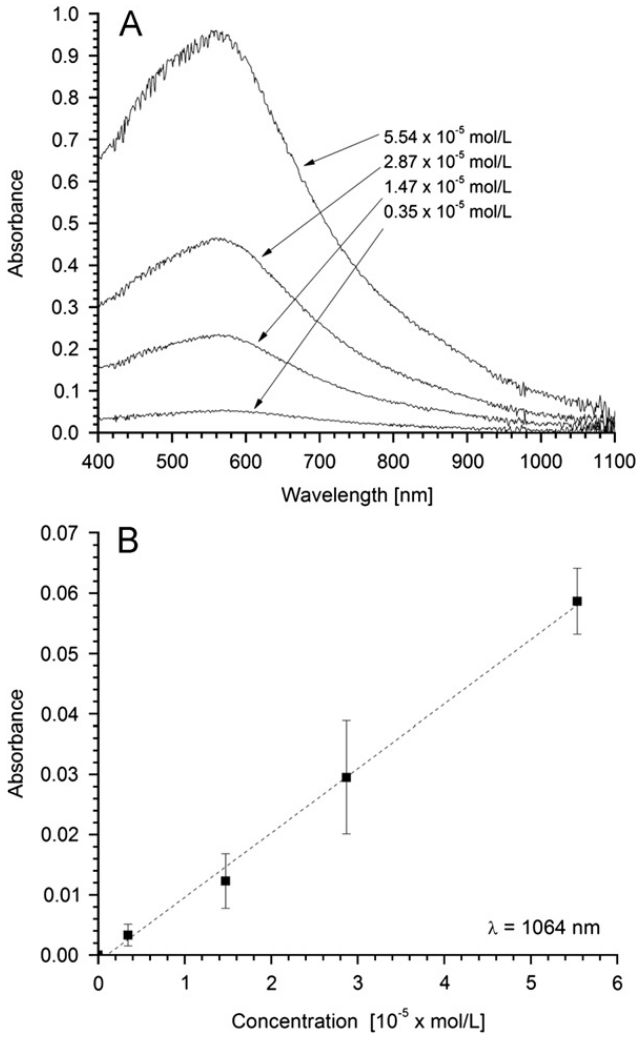

Fig. 8. Nigrosin absorbance of nigrosin mixed in de-ionized water with respect to (A) wavelength, and (B) molar concentration, as obtained from a UV/Vis spectrometer.

In this light, the contribution of absorption enhancement effects to the absorption measurements was estimated by comparing the isolated nigrosin and nigrosin/filter cases. Particle scattering was also assumed to be negligible ($\varepsilon_n=\alpha_n$). For the nigrosin/filter case, the reflectivity is significant ($\rho_{nf}=0.389\pm0.058$, where the subscript *nf* refers to the nigrosin-laden filter), but smaller than for the clean filter ($\rho_f=0.763\pm0.014$, where the subscript f refers to the clean filter), and is therefore indicative of both energy losses from the sample surface and possible scattering within the sample. Since $\rho_{nf}<\rho_f$, this may be an indication of the presence of enhanced absorption. Comparison of the absorption coefficient for the isolated nigrosin (given above) to that of the nigrosin/filter case, $\alpha_{nf}=(1.93\pm0.11)\times10^3\ m^{-1}$, resulted in a fivefold increase due the presence of the filter (similar to that found in the literature [13]).

4.2. Validation with packed nigrosin

The absorptivity of the packed nigrosin was determined from the LDTR measurements, and Eq. (18) was used to estimate the absorption coefficient. The following conditions were stipulated for the copper pan and determination of the nigrosin absorptivity. Since the probe beam impinges directly on the nigrosin within the pan, it is assumed that $I_{\rho,n}=I_{\rho,nc}$ where the subscripts *n*, *c*, and *nc* refer to the isolated nigrosin, clean copper pan, and nigrosin/pan cases, respectively. The transmissivity of the clean copper pan is negligible ($\tau_c=0$, considered as being optically opaque [42]), absorptivity is small (see Tables 2, $\beta_c=0.066\pm0.002$), and therefore the reflectivity is high [43]. The thermal conductivity is high (being of the same material as the copper reactor) and thus the pan

Table 4
Results of Lorenz–Mie calculations for a polydispersion of non-aggregated nigrosin particles dispersed within the volume of the filter. Inputs: $m_r=1.693+i0.275$, $\lambda=1.064\times10^{-6}$ m, $\tau_n=0.590$, $d=1.27\times10^{-3}$ m, $D_g=0.8\times10^{-7}$ m, and $\sigma_g=0.23$. The subscript $j=ext, sca, abs$, respectively.

	Extinction	Scattering	Absorption
Efficiency factor ($\overline{Q}_j$)	0.1377	0.0067	0.1310
Cross section ($\overline{C}_j$) (m^2)	0.7696×10^{-15}	0.0377×10^{-15}	0.7319×10^{-15}
Coefficient (ε, σ, α) (m^{-1})	414.8	20.3	394.5
Number density (N) (particles m^{-3})	0.5390×10^{18}		
Volume fraction ($\overline{C}_v$)	0.1833×10^{-3}		
Mean diameter (D_{32}) (m)	0.9131×10^{-7}		

acts to transmit thermal energy to the sample thermocouple. When the nigrosin is in the pan, the pan absorptivity is again negligible and the pan reflectivity ($\rho_n \approx 1$) is not sensed since the reflected incident radiation is off of the nigrosin (any possible pan reflectivity would be a secondary lower-order reflection reabsorbed by the nigrosin [29]). Because $\tau_c=0$, the transmissivity measurements need to be carried out either on the isolated sample or with an optically transparent container. Likewise, the pan needs to be thermally conductive to be used for the absorptivity measurements. Eq. (8) will hold true for each case, i.e., for the clean pan, nigrosin/pan, and isolated nigrosin. Eqs. (16) and (17) were used to isolate the effect of the pan and determine the isolated nigrosin optical characteristics. The results indicated that the nigrosin absorptivity was the same as that for the nigrosin/pan case (i.e., $\beta_n=\beta_{nc}$ since $\beta_c \approx 0$ for the nigrosin/pan case), $\rho_n=\rho_{nc}$, and $\tau_n=\tau_{nc}=\tau_c=0$. These results also satisfy Eq. (8) for self-consistency. As a result, the isolated nigrosin absorptivity was determined to be 0.956 ± 0.016 (from the LDTR measurements), as listed in Table 2, and the reflectivity off of the nigrosin surface will therefore be small.

To determine the absorption coefficient, we note again that the transmissivity of packed nigrosin is negligible ($\tau_n=0$). The absorbance and absorption coefficient (defined with respect to the absorption penetration depth) will then be relatively large (see Eq. (15)). To estimate a value for α_n, Eq. (18) is used along with the imaginary part of the refractive index and the aforementioned laser wavelength ($k=0.275 \pm 0.036$, $\lambda=1.064 \times 10^{-6}$ m). The value of k is derived from the above-mentioned Lorenz–Mie calculations for dispersed nigrosin particles, as confirmed from the agreement with the absorption measurements for the nigrosin-laden filters and the literature values listed in Table 1 for aerosolized nigrosin. It is assumed that the bulk refractive index remains unchanged from the aerosol values and uncorrected for wavelength since the difference would be less than the uncertainty in k (the wavelength dependence is assumed similar to that for carbon [44]). The resulting value for α_n is $(3.24 \pm 0.21) \times 10^6\ \mathrm{m}^{-1}$. If it is assumed that $\varepsilon_n=\alpha_n$ (for $\sigma_n \ll 1$, no internal scattering within the bulk substance), and $\tau_n=0$, then upon substitution into Eq. (10) the value for the absorption penetration depth (i.e., the distance over which absorption is estimated to occur) will be on the order of microns (i.e., using Eq. (13), $y=(1.16 \pm 0.23) \times 10^{-6}$ m for $k_c=2.5$). This result indicates that the absorption penetration depth of the packed opaque sample is consistent with the literature (e.g., Eckert and Drake [42], Siegel and Howell [32]).

4.3. Validation with nigrosin/de-ionized water suspensions

The nigrosin absorption coefficient for different molar concentrations of nigrosin mixed in de-ionized water, i.e., $(0.35,\ 1.47,\ 2.87,\ \text{and}\ 5.54) \times 10^{-5}\ \mathrm{mol\ L^{-1}} \pm 1.4 \times 10^{-7}\ \mathrm{mol\ L^{-1}}$, was determined with the LDTR and compared to UV/Vis spectrometer results. For the spectrometer, the nigrosin absorbance spectrum with regard to wavelength is presented in Fig. 8(A) (path length is 10.1 mm $\pm$ 0.013 mm) for each concentration (with the contribution of the de-ionized water removed by the instrument). The linear variation of the nigrosin absorbance with suspension molar concentration at a wavelength of 1.064×10^{-6} m (the wavelength of the probe beam for the LDTR experiments) is presented in Fig. 8(B). One can then determine the absorptivity from Eq. (8), knowing the measured absorbance, path length, and assuming negligible reflectivity (by the cuvette and particles, as is assumed by the instrument). For the nigrosin/de-ionized water suspension molar concentration of $5.54 \times 10^{-5}\ \mathrm{mol\ L^{-1}}$, the value of the nigrosin absorption coefficient from the UV/Vis spectrometer was $\alpha_n=(5.79 \pm 0.54)\ \mathrm{m}^{-1}$ ($\tau_n=0.943 \pm 0.002$ using $A^*=\alpha_n\ d$, $\beta_n=0.057 \pm 0.002$ for $\sigma_n=0$, and the water contribution was removed by referencing the measurements to clean de-ionized water). The LDTR experiments were carried out with the same nigrosin/de-ionized water suspension by filling a copper pan and carrying out the measurements for β_n at the aforementioned conditions. Transmissivity measurements (in the LDTR setup) were also carried out by placing the suspension in a polystyrene cuvette. Vaporization of the water over the course of the repeated experimental measurements made it difficult to measure the mass precisely and determine its uncertainty. The nigrosin absorption coefficient for this suspension (assuming negligible contribution by the pan, as discussed above) was $\alpha_n=(6.33 \pm 1.98)\ \mathrm{m}^{-1}$ ($\tau_n=0.938 \pm 0.019$ using $d=(10.1 \pm 0.013) \times 10^{-3}$ m for the transmissivity measurement, $\beta_n=0.062 \pm 0.008$ using $d=(2.34 \pm 0.008) \times 10^{-3}$ m for the LTDR measurement), and in good agreement with the above-mentioned UV/Vis spectrometer results. Note that the calculations included the weighted contribution for the specific heat capacity of water, and an average sample mass reduced about 58% from the initial value to account for water vaporization during heating. The contribution due to the de-ionized water and cuvette was removed according to Eqs. (16) and (17). As expected for a dilute suspension ($\rho_n=0$), $\beta_n \ll 1$, $\tau_n \longrightarrow 1$, and α_n is significantly smaller than the packed nigrosin values.

Comparing the different cases presented in Table 2, one finds that the nigrosin absorption coefficient increases with increasing nigrosin concentration, as expected. The absorption coefficient for the packed nigrosin in the copper pan has the largest value since the transmission was negligible. The nigrosin/filter case had the next largest value of α_n, and the nigrosin/de-ionized water suspension had the lowest concentration and thus the smallest absorption coefficient. The linearity in absorbance for the range of nigrosin-suspension concentrations presented in Fig. 8(B) does not extend to the relatively high nigrosin/filter and nigrosin/pan concentrations, as discussed earlier. The absorbance appears to increase in an exponentially decaying fashion with increasing concentration when comparing the suspension and filter cases, similar to results reported by Gundel et al. [45].

5. Summary

A laser-heating technique to measure absorptivity, in conjunction with transmissivity measurements, was used to determine the absorption coefficient of particle-laden quartz-fiber filters. The novelty of this approach is that it

overcomes measurement issues associated with other filter-based techniques. Validation of the approach was also carried out with packed particles in a copper pan and a nigrosin/de-ionized water suspension (which was also compared with results from a UV/vis spectrometer). The laser-heating methodology is based on perturbing the steady-state temperature of selected samples, with a probe laser beam directed at the sample, and monitoring the thermal response during decay back to the steady state. A theoretical model (based on thermal and electromagnetic radiation conservation) was used to evaluate the particle absorption coefficient.

The nigrosin absorption coefficient was estimated for nigrosin-laden quartz-fiber filters. The nigrosin absorption coefficient for the nigrosin/filter case compared favorably with an idealized dispersion of nigrosin particles within the volume of the filter, using Lorenz–Mie calculations for a polydispersion of particles (for which the distribution function was derived from DLS measurements of a nigrosin/de-ionized water suspension). It was also verified that the nigrosin scattering coefficient was small and that the influence of the filter on the nigrosin absorption coefficient (absorption enhancement) was significant. In addition, the packed nigrosin absorption coefficient was determined by estimating the imaginary part of the refraction index from the nigrosin/filter case, Lorenz–Mie calculations, and the literature. An absorption penetration depth was also defined and used to verify consistency with the literature. Measurements were carried out for a nigrosin/de-ionized water suspension at different concentrations, with favorable results obtained when compared to those from a UV/vis spectrometer.

Acknowledgments

The author would like to thank Dr. A. Nazarian for his assistance with the theory and operation of the laser-driven thermal reactor, Dr. J.T. Hodges for his insightful comments, Drs. S.D. Leigh and A.L. Rukhin for their assistance with the theory, Dr. J. Conny for the SEM images, Drs. G. Sanchez-Pomales and M.A. Pond for help with the DLS apparatus, Dr. A. Sedlacek for the nigrosin sample, and Ms. S. Hariri for her assistance while participating as a NIST Summer Undergraduate Research Fellow.

Appendix A

The polydispersion particle size distribution is represented by an assumed log-normal probability function,

$$P(D)=\frac{1}{\sqrt{2\pi}\sigma_g D}\exp\left\{\frac{-[\ln(D/D_g]^2}{2\sigma_g^2}\right\} \tag{A.1}$$

where D_g is the geometric mean diameter and σ_g is the geometric mean standard deviation. The procedure of Dobbins et al. [39,40] is used to evaluate the terms in Eq. (20), where $\overline{C}_j$ ($j=ext, sca, abs$) are the mean extinction, scattering, and absorption cross sections, respectively, $\overline{Q}_j$ ($j=ext, sca, abs$) are the mean extinction, scattering, and absorption efficiencies, respectively, $\overline{C}_v$ is the volume fraction, and D_{32} is the volume-to-surface area diameter (Sauter mean diameter), and are defined by:

$$\overline{C}_j=\frac{\pi}{4}\int_0^\infty Q_j[x,m_r(\lambda)]P(D)D^2\mathrm{d}D \tag{A.2}$$

$$\overline{Q}_j=\frac{4\overline{C}_j}{\pi\int_0^\infty P(D)D^2\mathrm{d}D} \tag{A.3}$$

$$\overline{C}_v=\frac{\pi}{6}N\int_0^\infty P(D)D^3\mathrm{d}D \tag{A.4}$$

$$D_{32}=\frac{\int_0^\infty P(D)D^3\mathrm{d}D}{\int_0^\infty P(D)D^2\mathrm{d}D} \tag{A.5}$$

where Q_j ($j=ext, sca, abs$) are the differential extinction, scattering, and absorption efficiencies for a specific particle (output from the Lorenz–Mie calculation [38]), respectively, x is the size parameter ($=\pi D/\lambda$), and $m_r(\lambda)$ is the complex refractive index ($=n_r+ik$). Equations (A.2)–(A.5) are transformed into simpler expressions by defining $z\equiv\ln(D/D_g)/\sqrt{2}\sigma_g$ before integrating over all particle sizes.

References

[1] Hansen ADA, Rosen H, Novakov T. The aethalometer – an instrument for the real-time measurement of optical absorption of aerosol particles. Sci. Total Environ. 1984;36:191–6.
[2] Fry ES, Kattawar GW, Pope RM. Integrating cavity absorption meter. Appl. Opt. 1992;31(12):2055–65.
[3] Campbell D, Copeland S, Cahill T. Measurement of aerosol absorption coefficient from teflon filters using integrating plate and integrating sphere techniques. Aerosol Sci. Technol. 1995;22(3):287–92.
[4] Lawless PA, Rodes CE, Ensor DS. Multiwavelength absorbance of filter deposits for determination of environmental tobacco smoke and black carbon. Atmos. Environ. 2004;38:3373–83.
[5] Bond TC, Anderson TL, Campbell D. Calibration and intercomparison of filter-based measurements of visible light absorption by aerosols. Aerosol Sci. Technol. 1999;30(6):582–600.
[6] Petzold A, Gysel M, Vancassel X, Hitzenberger R, Puxbaum H, Vrochticky S, Weingartner E, Baltensperger U, Mirabel P. On the effects of organic matter and sulphur-containing compounds on the CCN activation of combustion particles. Atmos. Chem. Phys. 2005;5:3187–203.
[7] Clarke AD. Effects of filter internal reflection coefficient on light absorption measurements made using the integrating plate method. Appl. Opt. 1982;21:3021–31.
[8] Bohren CF, Huffman DR. Absorption and Scattering of Light by Small Particles. New York, NY: Wiley; 1983 Chapters 2, 3, 11, and 14.
[9] Petzold A, Schönlinner M. Multi-angle absorption photometry – a new method for the measurement of aerosol light absorption and atmospheric black carbon. J. Aerosol Sci. 2004;35:421–41.
[10] Cappa CD, Lack DA, Burkholder JB, Ravishankara AR. Bias in filter-based aerosol light absorption measurements due to organic aerosol loading: evidence from laboratory measurements. Aerosol Sci. Technol. 2008;42(12):1022–32.
[11] Taha G, Box GP, Cohen DD, Stelcer E. Black carbon measurement using laser integrating plate method. Aerosol Sci. Technol. 2007;41:226–76.
[12] Conny, JM The optimization of thermal-optical analysis for the measurement of black carbon in regional PM2.5: a chemometric approach. EPA Report 600/R-07/119, U.S. Environmental Protection Agency, Office of Research and Development, Washington, DC, 2007.
[13] Bond TC, Bergstrom RW. Light Absorption by carbonaceous particles: an investigative review. Aerosol Sci. Technol. 2006;40(1):27–67.
[14] Randall, DA, Wood, RA, Bony, S, Colman, R, Fichefet, T, Fyfe, J, Kattsov, V, Pitman, A, Shukla, J, Srinivasan, J, Stouffer, RJ, Sumi A, and Taylor, KE Climate models and their evaluation. in: Climate

Change 2007: The Physical Science Basis. Contribution of Working Group I to the Fourth Assessment Report of the Intergovernmental Panel on Climate Change [Solomon, S. D Qin, M. Manning, Z. Chen, M. Marquis, K.B. Averyt, M. Tignor and H.L. Miller (Eds.)], Cambridge University, Cambridge, 2007.
[15] Sedlacek A, Lee J. Photothermal interferometric aerosol absorption spectrometry. Aerosol Sci. Technol. 2007;41:1089–101.
[16] Kondo Y, Sahu L, Kuwata M, Miyazaki Y, Takegawa N, Moteki N, Imaru J, Han S, Nakayama T, Oanh NTK, Hu M, Kim YJ, Kita K. Stabilization of the mass absorption cross section of black carbon for filter-based absorption photometry by the use of a heated inlet. Aerosol Sci. Technol. 2009;43(8):741–56.
[17] Justus BL, Kafafi ZH, Huston AL. Excited-state absorption-enhanced thermal optical limiting in C_{60}. Opt. Lett. 1993;18(19):1603–5.
[18] Justus BL, Huston AL, Campillo AJ. Broadband thermal optical limiter. Appl. Phys. Lett. 1993;63(11):1483–5.
[19] Radney JG, Bazargan MH, Wright ME, Atkinson DB. Laboratory validation of aerosol extinction coefficient measurements by a field-deployable pulsed cavity ring-down transmissometer. Aerosol Sci. Technol. 2009;43(1):71–80.
[20] Bazargan MH. Aerosol optical extinction measurements using a pulsed laser cavity-ring down transmissometer. Int. J. Chem. Technol. Res. 2009;1(3):394–400.
[21] Nakayama T, Kondo Y, Moteki N, Sahu LK, Kinase T, Kita K, Matsumi Y. Size-dependent correction factors for absorption measurements using filter-based photometers: PSAP and COSMOS. J. Aerosol Sci. 2010;41:333–43.
[22] Nazarian A, Presser C. Thermal and chemical kinetic characterization of multiphase and multicomponent substances by laser heating. Int. J. Heat Mass Transfer 2008;51(5–6):1365–78.
[23] Arnott WP, Moosmuller H, Rogers CF, Jin T, Bruch R. Atmos. Environ. 1999;33(17):2845–52.
[24] Lack DA, Lovejoy ER, Baynard T, Pettersson A, Ravishankara AR. Aerosol absorption measurement using photoacoustic spectroscopy: sensitivity, calibration, and uncertainty developments. Aerosol Sci. Technol. 2006;40(9):697–708.
[25] Spindler C, Riziq AA, Rudich Y. Retrieval of aerosol complex refractive index by combining cavity ring down aerosol spectrometer measurements with full size distribution information. Aerosol Sci. Technol. 2007;41(11):1011–7.
[26] Schnaiter M, Schmid O, Petzold A, Fritzsche L, Klein KF, Andrease MO, Helas G, Thielmnn A, Gimmler M, Möhler O, Linke C, Schurath U. Measurement of wavelength-resolved light absorption by aerosols utilizing a UV–vis extinction cell. Aerosol Sci. Technol. 2005;39(3):249–60.
[27] Taylor, B.N., and Kuyatt, C.E. Guidelines for evaluating and expressing the uncertainty of NIST measurement results. NIST Technical Note 1297, National Institute of Standards and Technology, Gaithersburg, MD, 1994.
[28] Haynes WM, et al., editors. CRC Handbook of Chemistry and Physics. 91st edn. Boca Raton, FL: CRC Press/Taylor and Francis; 2011 pp. 12–195 and 12–205.
[29] Incropera FP, DeWitt DP. Introduction to Heat Transfer. 4th edn. New York, NY: Wiley; 2001 pp. 248 and 516.
[30] Bass M, van Stryland EW, Williams DR, Wolfe WL, editors. Handbook of Optics. Optical Society of America. New York, NY: McGraw-Hill; 1995.
[31] Melton LA. Soot diagnostics based on laser heating. Appl. Opt. 1984;23(13):2201–8.
[32] Siegel R, Howell JR. Thermal Radiation Heat Transfer. 2nd edn. New York, NY: Hemisphere; 1981 Chapters 13 and 19.
[33] Liousse C, Cachier H, Jennings SG. Optical and thermal measurements of black carbon aerosol content in different environments: variation of the specific attenuation cross-section, sigma(s). Atmos. Environ., Part A 1993;27:1203–11.
[34] Weingartner E, Saathoff H, Schnaiter M, Streit N, Bitnar B, Baltensperger U. Absorption of light by soot particles: determination of the absorption coefficient by means of aethalometers. J. Aerosol Sci. 2003;34:1445–63.
[35] Harrison RM, van Grieken RE. Atmospheric Particles. New York: John Wiley; 1998 p. 114.
[36] Harris DC. Quantitative Chemical Analysis. 3rd edn. New York: Freeman and Company; 1991 Chapter 19.
[37] Skoog DA, Leary JJ. Principles of Instrumental Analysis. 4th edn. New York: Harcourt Brace College; 1991 Chapter 7.
[38] Wiscombe, WJ Mie Scattering Calculations: Advances in technique and fast, vector-speed computer codes. NCAR Technical Note 140+STR, National Center for Atmospheric Research, Boulder, CO, 1979.
[39] Dobbins RA, Crocco L, Glassman I. Measurement of mean particle sizes of sprays from diffractively scattered light. AIAA J. 1963;1(8):1882–6.
[40] Dobbins RA, Santoro RJ, Semerjian HG. Interpretation of optical measurements of soot in flames. Combustion diagnostics by nonintrusive methods. In: McKay JD, Roux JA, editors. Progress in Astronautics and Aeronautics, 92. American Institute of Aeronautics and Astronautics; 1984. p. 208–37.
[41] Presser C, Gupta AK, Semerjian HG, Santoro RJ. Application of laser diagnostic techniques for examination of fuel spray structure. Chem. Eng. Commun. 1990;90:75–102.
[42] Eckert ERG, Drake Jr RM. Analysis of Heat and Mass Transfer. New York: McGraw Hill; 1972 p. 598.
[43] Clark JA, editor. Theory and Fundamental Research in Heat Transfer. New York: Pergamon; 1963 pp. 12–15.
[44] Alexander. DTL, Crozier PA, Anderson JR. Brown carbon spheres in East Asian outflow and their optical properties. Science 2008;321:833–6.
[45] Gundel LA, Dod RL, Rosen H, Novakov T. The relationship between optical attenuation and black carbon concentration for ambient and source particles. Sci. Total Environ. 1984;36:197–202.
[46] Garvey DM, Pinnick RG. Response characteristics of the particle measuring systems active scattering aerosol spectrometer probe (ASASP-X). Aerosol Sci. Technol. 1983;2(4):477–88.
[47] Dinar E, Riziq AA, Spindler C, Erlick C, Kiss G, Rudich Y. The complex refractive index of atmospheric and model humic-like substances (HULIS) retrieved by a cavity ring down aerosol spectrometer (CRD-AS). Faraday Discuss. 2008;137:279–95.
[48] Riziq AA, Trainic M, Erlick C, Segre E, Rudich Y. Extinction efficiencies of coated absorbing aerosols measured by cavity ring down aerosol spectrometry. Atmos. Chem. Phys. 2008;8(6):1823–33.
[49] Lang-Yona N, Rudich Y, Segre E, Dinar E, Abo-Riziq A. Complex refractive indices of aerosols retrieved by continuous wave-cavity ring down aerosol spectrometer. Anal. Chem. 2009;81:1762–9.